

phys. stat. sol. (a) **107**, 775 (1988)

Subject classification: 61.60; 61.10; 61.16; S8

*Laboratoire de Chimie Minérale Structurale associé au C.N.R.S. U.A. 200,  
Faculté des Sciences Pharmaceutiques et Biologiques de Paris V<sup>1)</sup> (a)  
and C.E.C.M., Vitry<sup>2)</sup> (b)*

## X-Ray Diffraction and Electron Microscopy Studies of $\alpha$ - and $\beta$ -Ga<sub>2</sub>S<sub>3</sub>

By

A. TOMAS (a), M. GUYMONT (b), M. P. PARDO (a), M. GUITTARD (a),  
and J. FLAHAUT (a)

Dedicated to Prof. Dr. S. AMELINCKX on the occasion of his 65th birthday

Electron diffraction/microscopy and X-ray diffraction techniques are used to study the  $\alpha$ - and  $\beta$ -Ga<sub>2</sub>S<sub>3</sub> compounds. Diffuse streaks directed along [001]\* are related to a planar disorder described by three domain variants. The correspondence between domains is effected by rotations of  $2\pi/3$  and  $4\pi/3$  around the  $c$  hexagonal axis common to  $\alpha$  and  $\beta$  forms. Heating under electron beam leads to a significant structural change  $\alpha \rightarrow \alpha'$  directly observed in diffraction patterns and high resolution image.

Une description des structures des formes  $\alpha$  et  $\beta$  de Ga<sub>2</sub>S<sub>3</sub>, fondée sur les données de diffractions X et électronique est proposée. La présence de trainées diffuses parallèles à [001]\* visibles sur les diagrammes de diffraction X et électronique des formes  $\alpha$  et  $\beta$  est expliquée par un modèle faisant intervenir trois types de domaines se correspondant par des rotations de  $2\pi/3$  et  $4\pi/3$  autour de l'axe  $c$  hexagonal. Une interprétation de la transition de phases  $\alpha \rightarrow \alpha'$  obtenue par chauffage sous le faisceau d'électrons est proposée.

### 1. Introduction

The polymorphism of gallium sulfide Ga<sub>2</sub>S<sub>3</sub> has been demonstrated by several studies [1 to 4]. Four different phases are identified:  $\alpha$ -Ga<sub>2</sub>S<sub>3</sub> (hexagonal, space group P6<sub>1</sub> and P6<sub>5</sub>);  $\alpha'$ -Ga<sub>2</sub>S<sub>3</sub> (monoclinic, space group Bb);  $\beta$ -Ga<sub>2</sub>S<sub>3</sub> (hexagonal "wurtzite" structure P6<sub>3</sub>mc); and  $\gamma$ -Ga<sub>2</sub>S<sub>3</sub> (cubic "sphalerite" structure, F43m).

In the course of a general study of the phase diagram GaS-Ga<sub>2</sub>S<sub>3</sub> [5], mean crystal structures of  $\alpha$  and  $\beta$  forms have been determined, using an X-ray four-circle automatic diffractometer, on monocrystals having compositions Ga<sub>1-x</sub>S<sub>x</sub> close to Ga<sub>2</sub>S<sub>3</sub> ( $0.58 < x < 0.60$ ), neglecting diffuse scattering revealed by the careful examination of the reciprocal lattice [6].

The present paper is concerned with a description of the real structures of  $\alpha$ ,  $\alpha'$ , and  $\beta$  forms taking into account information carried by diffuse scattering, and based on new data obtained from electron diffraction and microscopy. Particularly, it was found that the  $\alpha$  form undergoes an order-disorder transition into  $\alpha'$  directly under the electron beam.

### 2. Crystal Structures of $\alpha$ , $\alpha'$ , and $\beta$ Forms

In each structure the S atoms are distributed in an almost perfect hexagonal close-packed array. Thus it is the arrangement of the Ga cations which causes the different structures  $\alpha$ ,  $\alpha'$ , and  $\beta$ .

<sup>1)</sup> 4, Avenue de l'Observatoire, F-75270 Paris Cédex 06, France.

<sup>2)</sup> 15, Rue G. Urbain, F-94400 Vitry, France.

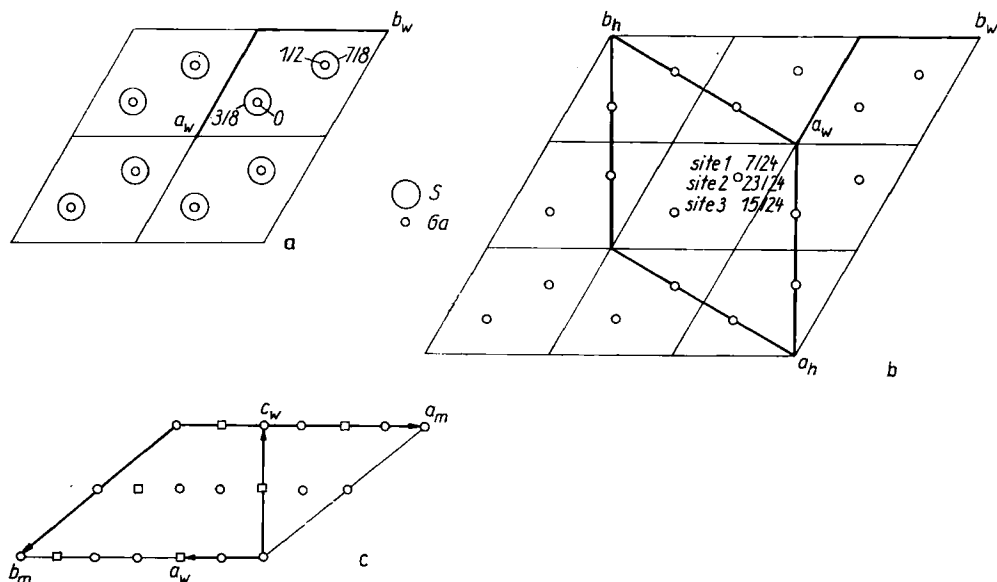


Fig. 1. a) Projection of the  $\beta$ - $\text{Ga}_2\text{S}_3$  wurtzite cell viewed along the  $c_w$ -axis,  $Z$  coordinates refer to  $c_w$  taken as unit (big circles S, small circles Ga). b) Projection of the  $\alpha$ - $\text{Ga}_2\text{S}_3$  cell along the  $c_h$ -axis. The "idealized" sites of Ga atoms ( $\circ$ ) and the relations between  $\beta$ - $\text{Ga}_2\text{S}_3$  substructure cell ( $a_w, b_w$ ) and  $\alpha$ - $\text{Ga}_2\text{S}_3$  superstructure cell ( $a_h, b_h$ ) are given. S atoms are not represented. c) Projection along the  $c_m$ -axis of the  $\alpha'$ - $\text{Ga}_2\text{S}_3$  cell ( $a_m, b_m$ ). The relation to the  $\beta$ - $\text{Ga}_2\text{S}_3$  cell ( $a_w, c_w$ ) is indicated ( $\circ$  Ga,  $\square$  vacancy)

The unit cell of the wurtzite-type  $\beta$ - $\text{Ga}_2\text{S}_3$ , with  $a_w = 0.3682(1)$  nm,  $c_w = 0.6031(2)$  nm, has its Ga atoms statistically distributed on  $2/3$  of the  $2b$  Wyckoff positions in space group  $P6_3mc$  (Fig. 1a).

Both  $\alpha$  and  $\alpha'$  forms are superstructures of the wurtzite-type due to ordering of the vacancies on cationic sites [2, 6, 7].

The hexagonal form  $\alpha$ - $\text{Ga}_2\text{S}_3$  ( $P6_1$  or  $P6_5$ ) has a unit cell  $a_h = 0.6385(1)$  nm,  $c_h = 1.8040(3)$  nm with 12 Ga atoms (Fig. 1b).

The monoclinic  $\alpha'$  form has a unit cell  $a_m = 1.1094(2)$  nm,  $b_m = 0.9578(2)$  nm,  $c_m = 0.6385(1)$  nm,  $\gamma = 141.15(1)^\circ$  and Ga atoms and vacancies are ordered on the  $4a$  Wyckoff positions of group Bb [7].

The relationship among the different cells is indicated on Fig. 1b and c. Neglecting the small distortion of the monoclinic  $\alpha'$  lattice, the following relations hold:

$$\begin{aligned} a_h &= a_w \sqrt{3}, & c_h &= 3c_w; \\ a_m &= 3a_w, & b_m &= \sqrt{(2a_w)^2 + c_w^2}, & c_w &= a_w \sqrt{3} = a_h. \end{aligned}$$

### 3. X-Ray Diffraction Observations

The observations were performed on crystals grown from mixtures  $\text{Ga}_2\text{S}_3 + \text{Ga}$  in different proportions, annealed 24 h at  $1000^\circ\text{C}$  in silica vacuum sealed ampoules, then quenched.

Laue and precession ( $\lambda = \text{MoK}\alpha$ ) photographs lead to the following remarks (Fig. 2a and b).

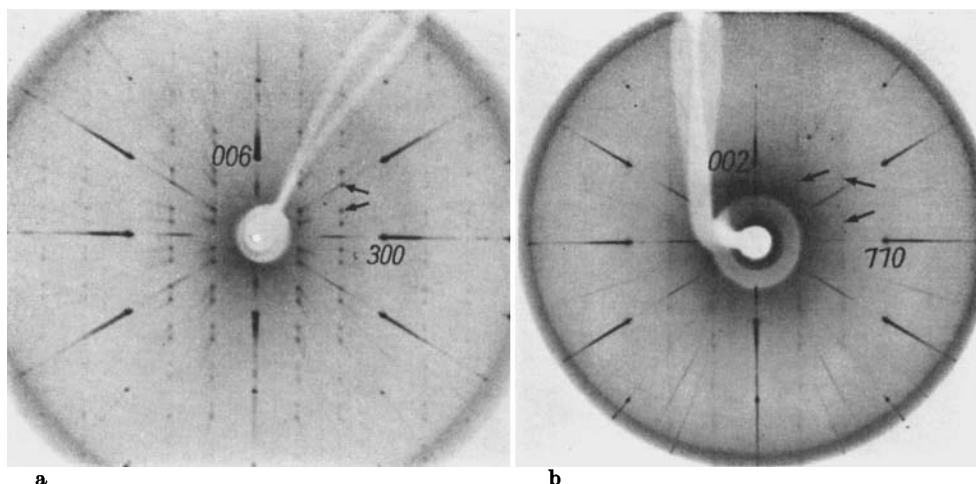


Fig. 2. a) X-ray precession of (010)\* reciprocal plane of  $\alpha$ -Ga<sub>2</sub>S<sub>3</sub>. Some superstructure reflections are indicated by arrows. Diffuse streaks joining these reflections are aligned along [001]\*. Indices refer to the ( $a_h^*$ ,  $c_h^*$ ) cell. b) X-ray precession of the equivalent ( $\bar{1}20$ )\* reciprocal plane of  $\beta$ -Ga<sub>2</sub>S<sub>3</sub> with indices referred to ( $a_w^*$ ,  $b_w^*$ ) cell. Superstructure reflections are now much more diffuse. Diffuse streaks indicated by arrows are clearly visible

1. For Ga<sub>1-x</sub>S<sub>x</sub> with  $0.59 \leq x \leq 0.595$ , therefore for compositions close to Ga<sub>2</sub>S<sub>3</sub>, the set of reflections is of Laue class 6/m and fulfils the condition  $00l$ ,  $l = 6n$ ; it corresponds to enantiomorphic space groups P6<sub>1</sub> or P6<sub>5</sub>. These reflections fall among two classes (Fig. 2a):

a) sharp reflections, whose  $h$ ,  $k$ ,  $l$  indices obey the relation:  $h, k, l = 3n$ ; this leads to a wurtzite-type cell of space group P6<sub>3</sub>mc;

b) more diffuse superstructure reflections of much smaller intensities, aligned in pairs and superimposed on diffuse streaks parallel to [001]\* with  $h \neq 3n$ .

2. For compositions with smaller values of  $x$  (away from Ga<sub>2</sub>S<sub>3</sub>) the intensities of diffuse streaks and of superstructure reflections considerably decrease, while the intensities of fundamental reflections remain unchanged (Fig. 2b).

#### 4. Interpretation of X-Ray Data

The determination of the mean structures of  $\alpha$  and  $\beta$  forms using a four-circle automatic diffractometer has been reported elsewhere [6]. The following conclusions are drawn:

(i) the optimised compositions obtained after refinement are Ga<sub>2.02</sub>S<sub>3</sub> for the  $\alpha$  form and Ga<sub>2.025</sub>S<sub>3</sub> for the  $\beta$  form. They are very close to each other;

(ii) in the  $\beta$  form, the distribution of Ga atoms is that of a wurtzite structure;

(iii) the  $\alpha$  form is a superstructure of  $\beta$  form obtained by a partial ordering of the twelve Ga atoms among the sites 1, 2, and 3 (see Fig. 1b) with occupation factors: 1, 0.67, and 0.35 [6]. Our conclusions are therefore different from those of Hahn and Frank [2] who found sites 1 and 2 completely occupied and site 3 empty, but are in agreement with those of Nguyen et. al. who find a partial occupation of sites 1, 2, and 3 [8]. The structure can be interpreted either as a statistical distribution of Ga atoms among the three sites, or as a structure consisting of three variants of fully ordered domains, each variant corresponding to the occupation of two of the sites (according

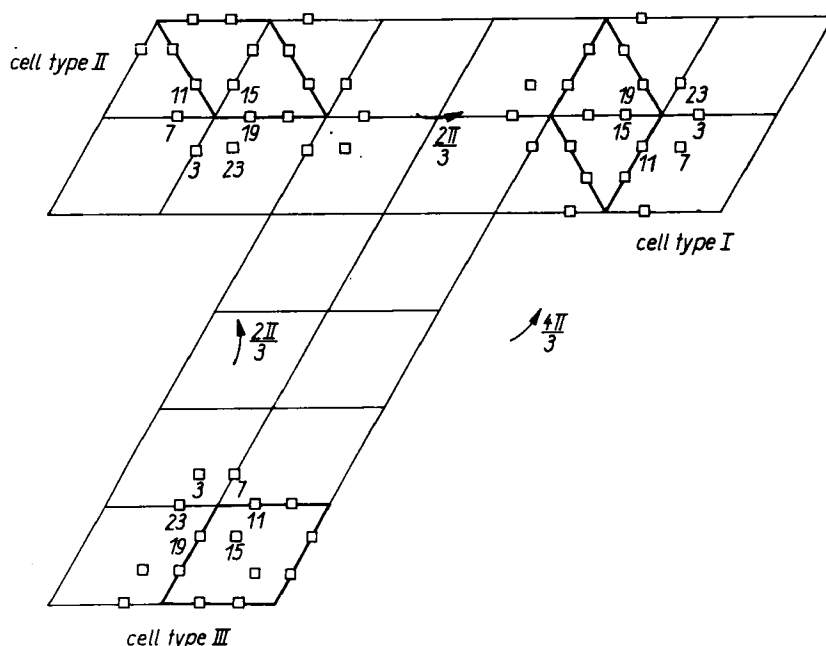


Fig. 3. Correspondence between the three domain variants indicated by three different cells (space group  $P6_1$ , description with enantiomorphic  $P6_5$  would be equivalent). The arrows correspond to boundary operators (rotations of  $2\pi/3$  or  $4\pi/3$  around  $c_h$ -axis). Only vacancies are drawn ( $\square$ ) and their "idealized"  $z$ -coordinates are given in  $c_h/24$  unit

to the Hahn-Frank description) and in such proportion as to give the overall statistical occupation.

This latter hypothesis is confirmed by the presence of diffuse streaks. Indeed a random cation distribution locally not very different from the overall distribution cannot give rise to anisotropic diffuse scattering (in other words, there is almost no shortrange ordering). On the other hand, the appearance of linear streaks implies the existence in the streak direction of a random stacking of ordered platelets (i.e. extended in directions perpendicular to the streak direction). These platelets are the ordered domains.

Therefore the  $\alpha$  form would consist of stacking of 65.3% domains where only sites 1 and 2 are occupied (variant III), 33.7% domains where only sites 1 and 3 are occupied (variant II), and 1% domains where only sites 2 and 3 are occupied (variant I). They all contribute in the same way to the sharp reflections of  $P6_1$  (or  $P6_5$ ) structure. As shown on Fig. 3, the correspondence between domains is effected by rotations of  $2\pi/3$  or  $4\pi/3$  around  $c_h$ . The boundary operators are thus  $3^1_{[001]}$  and  $3^2_{[001]}$ . Each boundary (interface) between domains would be a planar defect.

As  $x$  decreases in  $Ga_{1-x}S_x$  (i.e. the Ga proportion increases), the superstructure reflections become more diffuse and less intense while the basic reflections remain unchanged, which hints at a continuous transition from  $\alpha$  form to  $\beta$  form. This point will be discussed later (Section 6).

## 5. Electron Microscope Observations

All observations were performed on Jeol 200 CX operated at 200 kV.

### 5.1 Electron diffraction patterns

Electron diffraction along the [010] zone of several samples of  $\alpha$  and  $\beta$  forms has given three and only three types of diffraction patterns (Fig. 4a to c).

The diffraction pattern shown on Fig. 4a is similar to that obtained with the  $\alpha$  form by X-ray precession (Fig. 2a); outside fundamental reflections, pairs of superstructure spots, in general much less diffuse than on the corresponding X-ray pattern, are superimposed on streaks along the [001]\* direction. The streaks are reinforced between spots. The same patterns have always been obtained with the  $\beta$  structure.

Subsequent heating under the electron beam of the same sample leads to fading of these pairs of superstructure reflections and gives rise to the diffraction pattern of Fig. 4b. Diffuse scattering is clearly visible, superimposed on faint superstructure spots. After more heating, one is led to the diffraction pattern of Fig. 4c, on which diffuse scattering takes a centred connected net honeycomb-like shape, the fundamental reflections remaining unchanged. These diffraction patterns clearly correspond

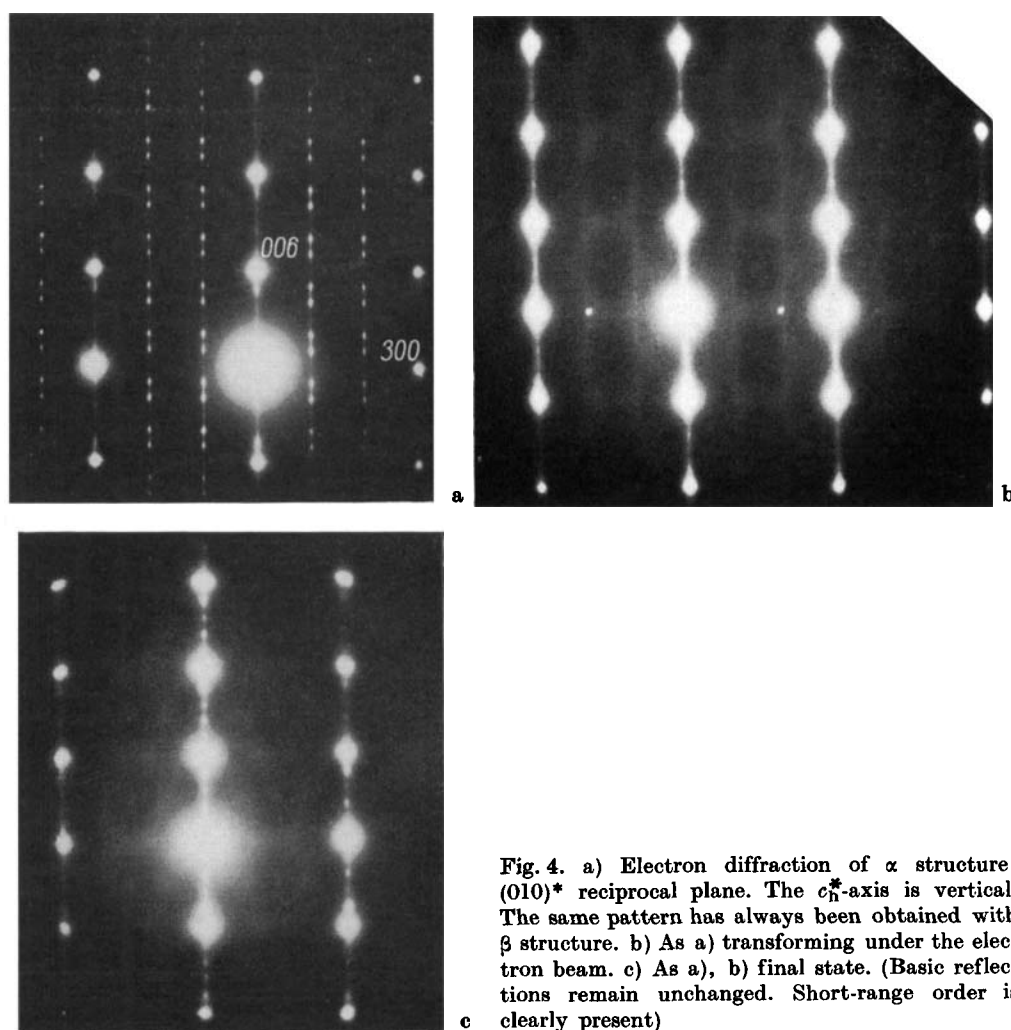


Fig. 4. a) Electron diffraction of  $\alpha$  structure: (010)\* reciprocal plane. The  $c_h^*$ -axis is vertical. The same pattern has always been obtained with  $\beta$  structure. b) As a) transforming under the electron beam. c) As a), b) final state. (Basic reflections remain unchanged. Short-range order is clearly present)

to a structure less ordered than  $\alpha$ , the one shown on Fig. 4b being an intermediary state. The phase transition is a disordering one, i.e. induced by a cation diffusion process; it is easily produced by heating and seems irreversible because the reverse transition (ordering) is much more sluggish.

At this stage, the sole inspection of the electron diffraction pattern of the final state of the transition does not allow to decide between  $\alpha'$  and  $\beta$  forms because the distortion due to the monoclinic lattice is too small. Imaging is needed.

### 5.2 Images

A dark field image obtained using one pair of superstructure spots (Fig. 5) shows a seemingly "random" distribution of planar defects, each defect being perpendicular to the direction of alignment of superstructure reflections.

A "more random" distribution of parallel planar defects is shown on another image (Fig. 6) where lattice fringes (bright field) reveal the defects by a variation of contrast.

A high resolution image of the  $\alpha$  structure attempted with an objective aperture collecting basic reflections with a number of surrounding superstructure spots has been obtained during the transformation of the  $\alpha$  form under the electron beam (as

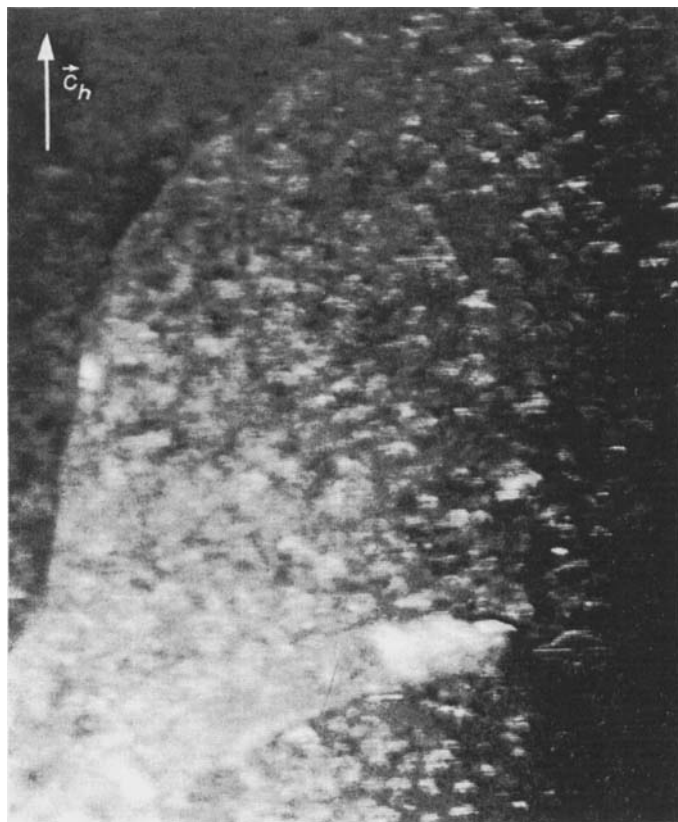


Fig. 5. Dark field image obtained with objective aperture enclosing two superstructure reflections of one pair. It is seen that each white area reveals fringes imaging the trace of planar defects all perpendicular to the reflection pair direction



Fig. 6. Lattice fringes (bright field) showing a random distribution of parallel planar defects

verified by turning back to the diffraction which was revealed to be similar to Fig. 4c) (Fig. 7). Due to the fluctuations of focussing during the transition, it has not been possible to maintain good astigmatism conditions in the whole area observed. The defects clearly reveal as interfaces between domains. The distance between two horizontal (i.e. along the interface direction) white dots is 0.54 nm exactly corresponding to the distance between two empty sites (Fig. 7 and 8). The angle between two directions of alignment of dots on each side of the interface is  $115^\circ$ , which agrees well with the angle between possible directions of alignment of vacancy sites (see Fig. 8). The distance between two successive white dots running along one of these directions of alignment is about 0.31 nm.

## 6. Interpretation of the Observations

X-ray (Fig. 2a) and electron diffraction (Fig. 4) patterns are identical for the  $\alpha$  form but differ in the diffuseness and intensity of superstructure spots for the  $\beta$  form (Fig. 2b and 4). This discrepancy is only apparent if we admit that the so-called

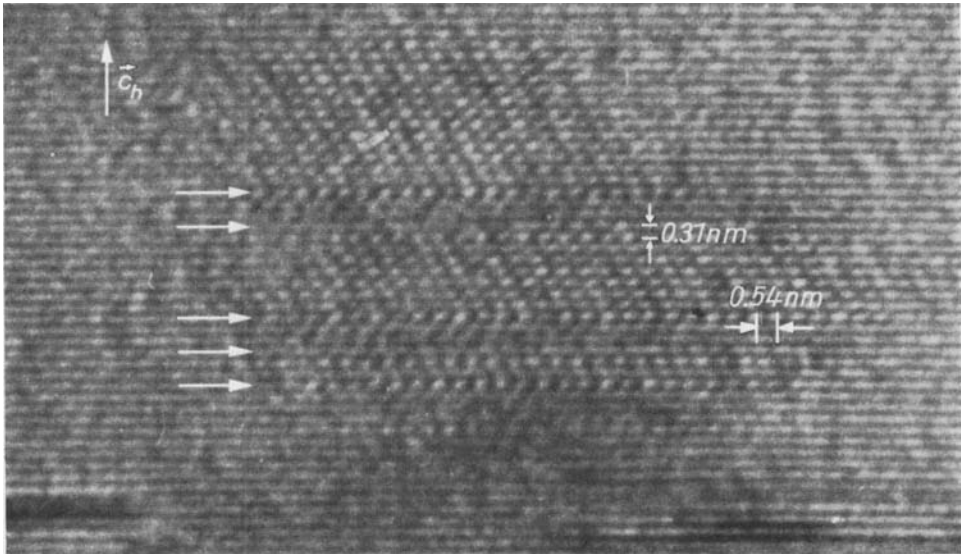


Fig. 7. High resolution image of the  $\alpha$  form while transforming (see text). Each planar defects is an interface between domains indicated by white arrows

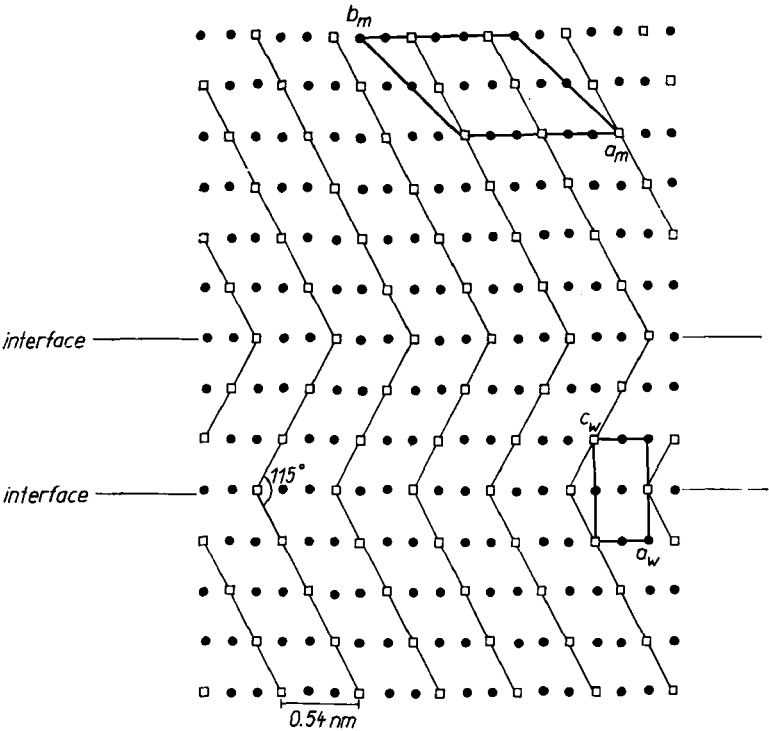


Fig. 8. Projected structure corresponding to Fig. 7 (● Ga, □ vacancy)



$\beta$  form is built with domains which retain the same structure as in the  $\alpha$  form but with a greater fluctuation in thickness around the mean value.

All the domains of the crystal interact with the X-ray beam to give a diffraction pattern with sharp substructure reflections and very diffuse weak superstructure spots (Fig. 2b) which, the latter being neglected, leads to a statistical wurtzite-type P6<sub>3</sub>mc structure. The electron beam, having a much smaller cross section, interacts only with a few domains, thus giving rise to a diffraction pattern with sharp basic and superstructure reflections quite similar to the one obtained for the  $\alpha$  form (Fig. 2a).

As the Ga proportion increases the fluctuation of domain thickness around the mean value becomes greater and an observation of X-ray patterns of the [010]\* plane shows that the intensities of the superstructure reflections considerably decrease.

As shown on Fig. 9 the  $\alpha$  form is built as a regular stacking of alternative layers E and F, the vacancies displaying a helicoidal arrangement. The  $\alpha'$  form is built up with a stacking of only one type of layers E and the vacancies are aligned in projection along the [110] monoclinic direction [7]. Equivalent monoclinic structure would be obtained with stacking of only F layers, vacancies being aligned now in the [130] monoclinic direction.

The high resolution image (Fig. 7) does not reveal an "ideal" monoclinic form as described by Collin et. al. [7] but rather a twinned monoclinic structure associating the two possible projected vacancy directions ([110] mono and [130] mono).

The honeycomb-like shape diffuse scattering shown on Fig. 6 is due to a short-range order probably related to a local composition [9] whose study is in progress.

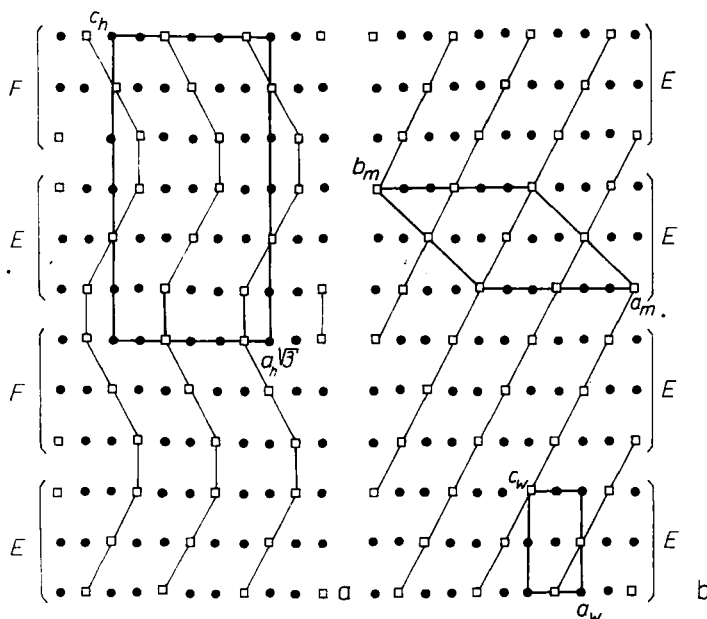


Fig. 9. a) Projection along the  $b_h$ -axis of the  $\alpha$ -Ga<sub>2</sub>S<sub>3</sub> structure. b) Projection along the  $c_m$ -axis of the  $\alpha'$ -Ga<sub>2</sub>S<sub>3</sub> structure. S atoms are not represented. The relations between  $(a_w, c_w)$  cell and  $(a_h, c_h)$  or  $(a_m, b_m)$  cells are represented (● Ga, □ vacancy)

### References

- [1] H. HAHN and W. KLINGLER, Z. anorg. allg. Chem. **259**, 135 (1949).
- [2] H. HAHN and G. FRANK, Z. anorg. allg. Chem. **278**, 333 (1955).
- [3] J. GOODYEAR, W. J. DUFFIN, and G. A. STEIGMANN, Acta cryst. **14**, 1168 (1961).
- [4] J. GOODYEAR and G. A. STEIGMAN, Acta cryst. **16**, 946 (1963).
- [5] M. P. PARDO, A. TOMAS, and M. GUITTARD, Mater. Res. Bull., in the press.
- [6] A. TOMAS, M. P. PARDO, and M. GUITTARD, Mater. Res. Bull. **22**, 1549 (1987).
- [7] G. COLLIN, J. FLAHAUT, M. GUITTARD, and A. M. LOIREAU-LOZAC'H, Mater. Res. Bull. **11**, 285 (1976).
- [8] NGUYEN HUY DUNG, M. P. PARDO, and L. DOGGUY-SMIRI, Mater. Res. Bull. **17**, 293 (1982).
- [9] R. DE RIDDER, G. VAN TENDELOO, and S. AMELINCKX, Acta cryst. **A32**, 216 (1976).

*(Received March 29, 1988)*